Chinese Chemical Letters 34 (2023) 107877

Contents lists available at ScienceDirect

Chinese Chemical Letters

journal homepage: www.elsevier.com/locate/cclet

Synthesis of stimuli-responsive pillararene-based supramolecular polymer materials for the detection and separation of metal ions

Yongfu Li[a,1], Xinyue Lou[a,1], Chunyu Wang[b], Yan Wang[a,*], Yu Jia[c], Qi Lin[c], Yingwei Yang[a,*]

[a] International Joint Research Laboratory of Nano-Micro Architecture Chemistry, College of Chemistry, Jilin University, Changchun 130012, China
[b] State Key Laboratory of Supramolecular Structure and Materials, Institute of Theoretical Chemistry, Laboratory of Theoretical and Computational Chemistry, College of Chemistry, Jilin University, Changchun 130012, China
[c] Key Laboratory of Eco-Functional Polymer Materials of the Ministry of Education, Key Laboratory of Eco-Environmental Polymer Materials of Gansu Province, College of Chemistry and Chemical Engineering, Northwest Normal University, Lanzhou 730070, China

ARTICLE INFO

Article history:
Received 7 July 2022
Revised 29 September 2022
Accepted 2 October 2022
Available online 13 October 2022

Keywords:
Aggregation-induced emission
Host–guest chemistry
Sensing and separation
Stimuli-responsive materials
Supramolecular polymer materials

ABSTRACT

A stimuli-responsive supramolecular polymer network (G-$(CN)_2$⊂BXDSP5) with aggregation-induced emission (AIE) properties has been efficiently constructed by host–guest interactions between pillar[5]arene derivative BXDSP5 and a homoditopic guest G-$(CN)_2$, which shows not only excellent fluorescence properties due to the AIE effect but also desirable ion-sensing abilities in both solution and solid states, holding great potential in the applicable fluorescence detection for Fe^{3+}. The resultant G-$(CN)_2$⊂BXDSP5 can be transformed into supramolecular polymer gel at high concentration *via* multiple noncovalent interactions, showing multi-stimuli-responsiveness in response to temperature change, mechanical force, and competitive agent. Meanwhile, the xerogel of supramolecular polymer material has been successfully used to remove Fe^{3+} from water with high adsorption efficiency. In addition, an ion-responsive film based on supramolecular polymer has also been developed, which can serve as a practical and convenient fluorescence test kit for detecting Fe^{3+}.

The detection and separation of hazardous metal ions such as Fe^{3+} are seminal in environmental protection and healthcare [1,2]. So far, fluorescence sensing has been considered one of the most powerful and convenient strategies for qualitatively and quantitatively measuring metal ions because of its multiple superiorities, including high sensitivity and efficiency, low cost, and easy operation [3–5]. Particularly, fluorescent supramolecular systems comprising organic luminophores and supramolecular functional groups that can be assembled *via* noncovalent interactions, possessing abundant recognition sites and tunable luminescent properties, have attracted tremendous attention in fluorescence detection and supramolecular sensing [6,7]. Although much progress has been made in the construction and application of fluorescent supramolecular materials, advantages, including optimized emission properties and good sensing ability of the materials in both solution and the solid phases, are still under extensive pursuit by researchers.

Aggregation-induced emission (AIE) [8], an intriguing photophysical phenomenon where the fluorophores show very weak or no fluorescence in dilute solutions but exhibit dramatically enhanced emission in the aggregated or solid states due to the restriction of intramolecular motion, has aroused extensive attention and experienced flourishing progress in numerous fields spanning from material science to biotechnology [9,10]. Among numerous AIE materials, AIE supramolecular polymers have been constructed as polymeric arrays of small AIE-active molecular units connected by noncovalent interactions [11–13]. Because of the dynamic and reversible nature of noncovalent interactions, AIE supramolecular polymers are highly responsive to certain external stimuli, such as temperature changes [14], pH variations [15], redox [16], ions [17], light [18] and mechanical forces [19], and their tunable physicochemical and photophysical properties endow them with application potentials in sensors [20], cellular imaging [21], artificial light-harvesting [22], drug release [23], and display or storage device [24].

Pillar[*n*]arenes (pillararenes), as a class of supramolecular macrocyclic hosts with rigid pillar-shaped architectures and electron-rich cavities [25–27], are superior candidates for constructing multi-functional supramolecular assembly systems with tunable topological structures and properties [28–32]. Up till now, pillararene-based stimuli-responsive supramolecular polymers have been applied in many areas, such as fluorescence

* Corresponding authors.
E-mail addresses: ywyang@jlu.edu.cn (Y. Wang), wangy2011@jlu.edu.cn (Y. Yang).
[1] These authors contributed equally to this work.

https://doi.org/10.1016/j.cclet.2022.107877
1001-8417/

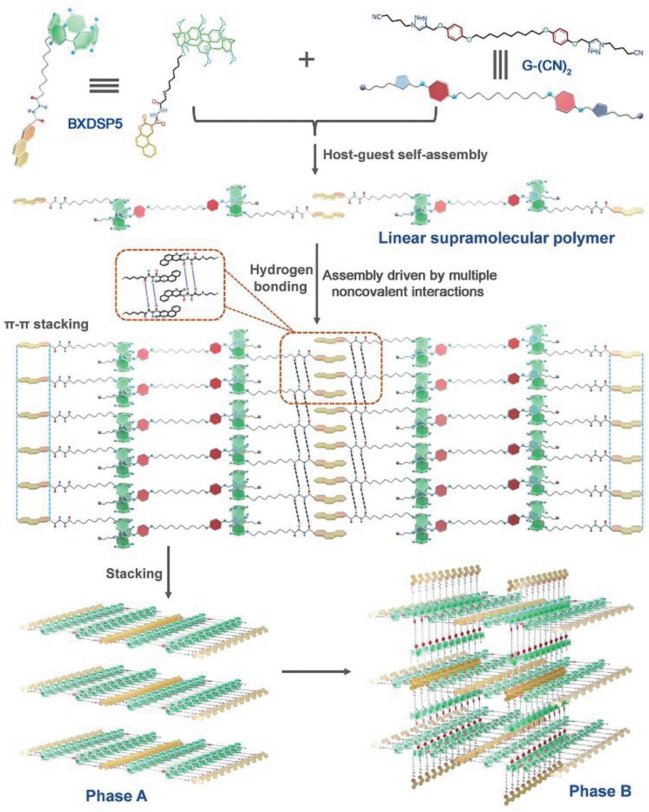

Fig. 1. Chemical structures of BXDSP5 and G-$(CN)_2$ and the schematic representation of the assembly process of supramolecular polymer G-$(CN)_2$⊂BXDSP5.

sensing, intelligent materials, molecular switches, and artificial light-harvesting systems [33–37]. Enlightened by these considerations and our previous studies on functionalized macrocycle-based supramolecular materials [38–42], we report a facile approach to construct a new stimuli-responsive supramolecular polymer, G-$(CN)_2$⊂BXDSP5, which exhibits a superior ability of selective and quantitative detection of Fe^{3+} in both solution and gelation by dramatic luminescence change. The metal coordination of the monofunctionalized pillar[5]arene BXDSP5 and Fe^{3+} results in the formation of the non-luminescent complex G-$(CN)_2$⊂BXDSP5@Fe^{3+}. The AIE supramolecular network G-$(CN)_2$⊂BXDSP5 can be transformed into supramolecular gel at a high concentration, which possesses multi-stimuli-responsive properties and can adsorb Fe^{3+} from water with excellent adsorption efficiency under the state of xerogel. Hence, we envision that this work will significantly extend the application of pillararene-based fluorescent supramolecular materials in selective sensing and visual detection.

The synthetic procedures of the target host compound (BXDSP5), guest compound (G-$(CN)_2$), and model guest (GM-CN) are provided in Schemes S1 and S2 (Supporting information). The target host and guest compounds and main precursors were fully characterized by ^{1}H NMR, ^{13}C NMR, and mass spectroscopy (Figs. S1–S25 in Supporting information). In the fabrication of the stimuli-responsive supramolecular polymer material, the pillararene derivative (BXDSP5) bearing one benzo[*f*]coumarin moiety can serve as the π-π stacking site and the emissive center, associated by a neutral guest G-$(CN)_2$ *via* host–guest recognition and π-π stacking to form a linear supramolecular polymer (Fig. 1).

To verify the host–guest interaction that drove the supramolecular polymerization process, measurements including ^{1}H and 2D DOSY NMR, 2D ROESY NMR, scanning electron microscopy (SEM), and dynamic light scattering (DLS) were performed. First, 2D ROESY NMR spectra of BXDSP5 were obtained to eliminate the self-inclusion of the benzo[*f*]coumarin-bearing side chain in the pillararene cavity. The ROE correlations of the protons H_b, H_d, H_e, H_f, H_h, H_i, H_j and H_m were observed, attributing to the π-π stacking of the arms at high concentrations (Fig. 2A). However, no such signals have been found between the alkyl chain and aromatic and/or the bridging methylene protons of the pillararene moiety, which strongly confirmed that there was no inclusion complexation in one BXDSP5 molecule. To further confirm the host–guest interaction, we used the model compound DMP5 and GM-CN to replace host molecule BXDSP5 and guest molecule G-$(CN)_2$, respectively, which could effectively prevent the overlap between the signals of the alkyl protons on BXDSP5 and G-$(CN)_2$. A slow exchange process emerged because of the host–guest complexation of DMP5 and GM-CN, and the alkyl proton signals of GM-CN in the presence of DMP5 also displayed a considerable upfield shift (Fig. 2B), indicating that GM-CN was included in pillararene cavity. For DMP5, the observable downfield shifts of H_α and H_β also confirmed the complexation. The ^{1}H NMR spectrum of BXDSP5 and G-$(CN)_2$ also suggested host–guest complexation (Fig. S26 in Supporting information). In addition, weight-average diffusion coefficients (D) of BXDSP5 and G-$(CN)_2$⊂BXDSP5 were measured to be 1.15×10^{-9} and 8.05×10^{-10} m^2/s, suggesting the formation of larger aggregates (Fig. 2C). Besides, DLS measurements of BXDSP5, G-$(CN)_2$, and BXDSP5 with G-$(CN)_2$ were also conducted in DMSO-H_2O binary solution (v/v, 1:9) to explore the size distribution profile of the formed aggregates. The mixture of BXDSP5 and G-$(CN)_2$ at the concentration of 0.02 mmol/L showed average hydrodynamic diameter values of 68.1 nm and 50.7 nm, respectively, while the mixed solution of BXDSP5 and G-$(CN)_2$ with a molar ratio of 2:1 possessed a mean diameter distribution centered at 91.3 nm, suggesting the transformation from small aggregates to bulky supramolecular polymers (Fig. 2D). Furthermore, fluorescence enhancement of G-$(CN)_2$⊂BXDSP5 was observed as compared with BXDSP5 (Fig. 2E), attributing to supramolecular assembly-induced emission enhancement [43] and proving the supramolecular assembly.

Moreover, the 2D ROESY NMR spectrum of G-$(CN)_2$⊂BXDSP5 verified the inclusion complexation of BXDSP5 and G-$(CN)_2$, revealing that the cyanoalkyl units of G-$(CN)_2$ were included in the pillararene cavity and stabilized by multiple C-H···π interactions and C-H···O interactions and the π-π stacking interactions of adjacent host molecules (Fig. S27 in Supporting information). SEM studies indicated that microspheres were formed in dilute DMSO-H_2O mixed solvents of both BXDSP5 and G-$(CN)_2$, attributing to the hydrophobic effect. The SEM image of G-$(CN)_2$⊂BXDSP5 suggested the structures of overlapped layers (Fig. S28C in Supporting information), reflecting morphology transformation to generate cross-linked 2D networks.

To gain a deeper understanding of the host–guest interaction mechanism of G-$(CN)_2$⊂BXDSP5, the electrostatic surface potential (ESP) maps, optimized structures, and frontier molecular orbitals (HOMO and LUMO) as well as energy gaps (ΔE) of BXDSP5, G-$(CN)_2$ and G-$(CN)_2$⊂BXDSP5 were obtained. The cyanobutoxyl moieties of G-$(CN)_2$ show electron-deficient characteristics, endowing them with a strong tendency to interact with electron-rich species. Meanwhile, the electron-rich pillararene entity of BXDSP5 largely favors the formation of host–guest complexes (Fig. S29A in Supporting information). Furthermore, the proposed binding mode was verified by the optimized structure of G-$(CN)_2$⊂BXDSP5 (Tables S3 in Supporting information). The HOMO of BXDSP5 is uniformly located in the cavity, while its LUMO extends over the benzo[*f*]coumarin group. In contrast, the HOMO of G-$(CN)_2$⊂BXDSP5 lies on the side of the pillar [5] arene rings. Moreover, the energy gap (ΔE) of G-$(CN)_2$⊂BXDSP5 is smaller than both that of BXDSP5 and G-$(CN)_2$ (Fig. S29B in Supporting information), suggesting that the host–guest complexation between

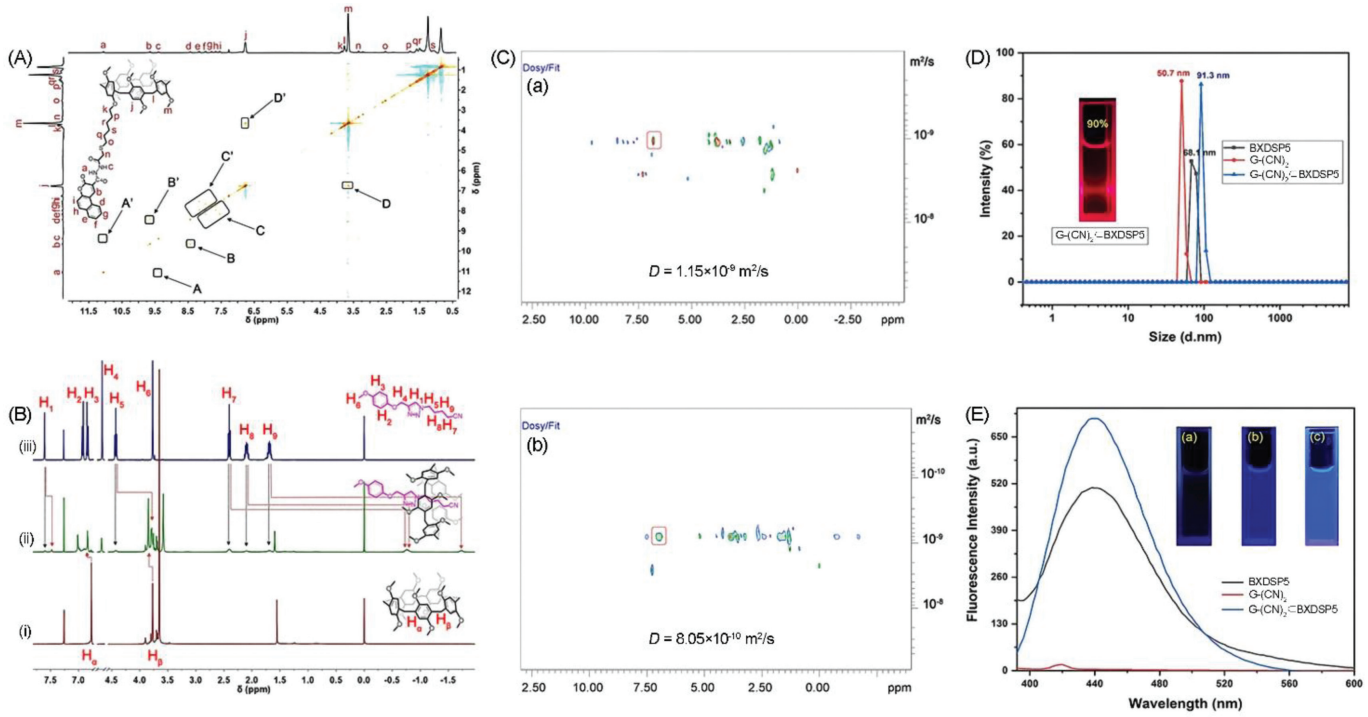

Fig. 2. (A) Partial spectrum of 2D ROESY spectrum (600 MHz, $CDCl_3$, 298 K) of BXDSP5 (20 mmol/L) with a mixing time of 200 ms. (B) ^{1}H NMR spectra (400 MHz, $CDCl_3$, 298 K) of (i) DMP5 (10 mmol/L), (ii) DMP5⊂GM-CN 1:1 mixture (10 mmol/L) and (iii) GM-CN (10 mmol/L). (C) 2D DOSY spectra (600 MHz, $CDCl_3$, 298 K) of (a) 4 mmol/L host BXDSP5 and (b) supramolecular polymer G-$(CN)_2$⊂BXDSP5 (4 mmol/L, 1:2 mixture). (D) DLS profiles of BXDSP5 (0.02 mmol/L), G-$(CN)_2$ (0.02 mmol/L), and G-$(CN)_2$⊂BXDSP5 (0.02 mmol/L) in a DMSO-H_2O mixed solution (DMSO:H_2O = 1:9) at 298 K. Inset: digital photograph presenting the Tyndall effect of supramolecular polymer. (E) Fluorescent spectra of G-$(CN)_2$, BXDSP5, and G-$(CN)_2$⊂BXDSP5. Inset: photographs displaying the fluorescence changes of (a) G-$(CN)_2$, (b) BXDSP5 and (c) G-$(CN)_2$⊂BXDSP5 under a UV lamp. (Experimental conditions: λ_{ex} = 365 nm; slit widths: Ex. 5 nm, Em. 5 nm; [BXDSP5] = 40 μmol/L, [G-$(CN)_2$] = 20 μmol/L, and [G-$(CN)_2$⊂BXDSP5] = 20 μmol/L G-$(CN)_2$ with 40 μmol/L BXDSP5 in DMSO-H_2O (5:95, v/v) as solvent, 298 K).

G-$(CN)_2$ and BXDSP5 is highly favored by forming supramolecular assemblies with more stable energy states [44].

To gain insight into the construction of the supramolecular polymer network and the self-assembly behavior in solution, concentration-dependent ^{1}H NMR spectra of G-$(CN)_2$⊂BXDSP5 were performed over a concentration range of 1.0–90.0 mmo/L (Fig. 3A). As the monomer concentration increased, the proton signals of H_b, H_d, H_e, H_f, H_g, H_h and H_i of BXDSP5 underwent substantial upfield shifts. Meanwhile, H_a and H_c experienced considerable downfield shifts, implying that intermolecular hydrogen bonding and π-π interactions were involved in the supramolecular polymerization. Meanwhile, the signals of H_7, H_9, and H_{10} of the cyanoalkyl groups shifted upfield and were accompanied by downfield shifts of the protons H_j and H_l from BXDSP5, indicating that the host–guest interactions were enhanced during host–guest self-assembly. In addition, all the signals broadened markedly at high concentrations, which is characteristic of a supramolecular polymer with high molecular weight [45]. On the other hand, the absorbance of G-$(CN)_2$⊂BXDSP5 (20 μmol/L) slightly decreased with an elevated temperature (Fig. 3B), also indicating the existence of hydrogen bonding owing to the temperature-dependent features [46]. Wide-angle PXRD was tested to demonstrate the molecular packing of G-$(CN)_2$⊂BXDSP5 (Fig. S30 in Supporting information). 2D DOSY NMR experiments were conducted to probe the aggregation of G-$(CN)_2$⊂BXDSP5 during supramolecular polymerization. The weight average diffusion coefficient (D) in $CDCl_3$ solution decreased significantly from 11.10×10^{-10} m^2/s to 6.99×10^{-11} m^2/s as G-$(CN)_2$⊂BXDSP5 concentration increased from 1 mmol/L to 90 mmol/L (Fig. 3C), signifying a high degree of supramolecular polymerization. Thus, the above experiments provide detailed information that the monomers assembled into an extended polymeric structure assisted by the synergetic effect of multiple noncovalent interactions and highlight the concentration dependence of supramolecular polymerization (Fig. 1).

Interestingly, the emission of this constructed supramolecular polymer G-$(CN)_2$⊂BXDSP5 at 440 nm was extremely weak in pure DMSO, but the fluorescence showed a sudden increase as the water (poor solvent) fraction was higher than 80% (Figs. S31A and B in Supporting information). Upon gradual increasing the H_2O fraction (over 80%) to DMSO containing BXDSP5 and G-$(CN)_2$, a Tyndall effect was observed, suggesting supramolecular polymerization and colloidal aggregation (Fig. S31C). These results indicate that the fluorescence emission of the supramolecular polymer could be credited to the well-established AIE mechanism. With the water content gradually increased, the degree of aggregation of supramolecular polymers was greatly improved, which contributed to the restriction on the innate rotation of G-$(CN)_2$⊂BXDSP5 by the collaboration of multiple noncovalent interactions, causing the blockage of nonradiative pathways and the promoted radiative channels. More importantly, the fluorescence of G-$(CN)_2$⊂BXDSP5 showed excellent stability (Fig. S31D in Supporting information). Simultaneously, the fluorescence quantum yield (Φ) and lifetime (τ) of this AIE supramolecular polymer were measured to be 14.11% and 3.56 ns, respectively (Figs. S32A and S32B in Supporting information).

The luminescent responses of supramolecular polymer G-$(CN)_2$⊂BXDSP5 toward various cations, including Fe^{3+}, Hg^{2+}, Zn^{2+}, Pb^{2+}, Cu^{2+}, Cd^{2+}, Ni^{2+}, Co^{2+}, Ca^{2+}, Ag^{+}, Mg^{2+}, Cr^{3+}, Ba^{2+}, Na^{+}, K^{+} and Al^{3+}, were investigated in DMSO-H_2O mixed solvents (1:9, v/v). Interestingly, among all tested metal ions added to G-$(CN)_2$⊂BXDSP5, only Fe^{3+} showed an obvious fluorescence suppression, which could be observed clearly with naked eyes when the sample solutions were irradiated under UV light of 365 nm, indicating that the supramolecular polymer could effectively detect Fe^{3+} with excellent selectivity (Fig. 4A). Furthermore,

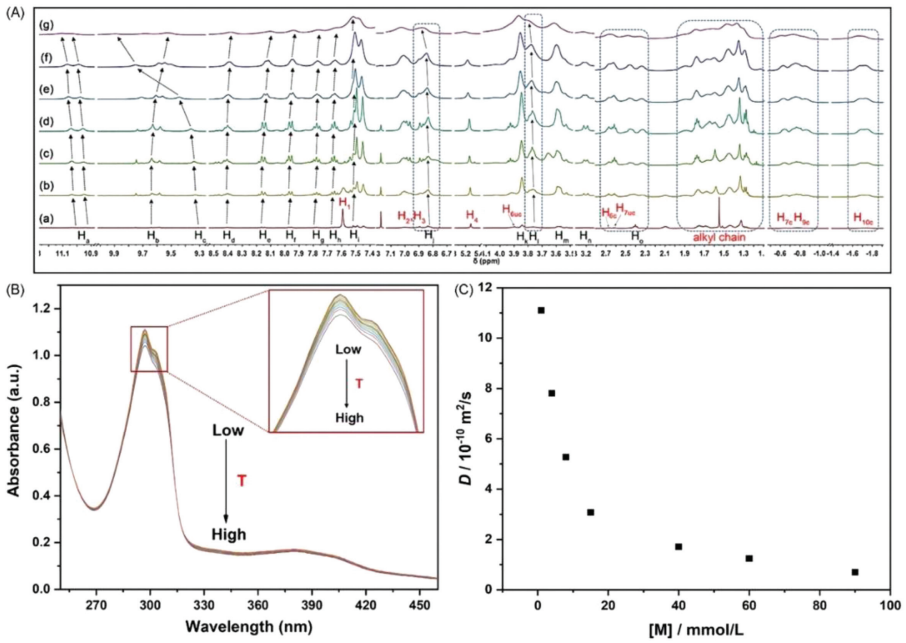

Fig. 3. (A) The partial ^{1}H NMR spectra ($CDCl_3$, 298 K, 400 MHz) of G-$(CN)_2$⊂BXDSP5 at different concentrations (from bottom to top: 1, 4, 8, 15, 40, 60 and 90 mmol/L. Peaks of uncomplexed monomers and supramolecular complexes are designated as uc and c, respectively. (B) Absorbance spectra of G-$(CN)_2$⊂BXDSP5 (20 μmol/L) at different temperatures in DMSO-H_2O (v/v = 1/9) binary solution. (C) Concentration-dependent diffusion coefficient D (from ^{1}H NMR spectroscopy 600 MHz, $CDCl_3$, 298 K) of G-$(CN)_2$⊂BXDSP5 (1:2 mixture).

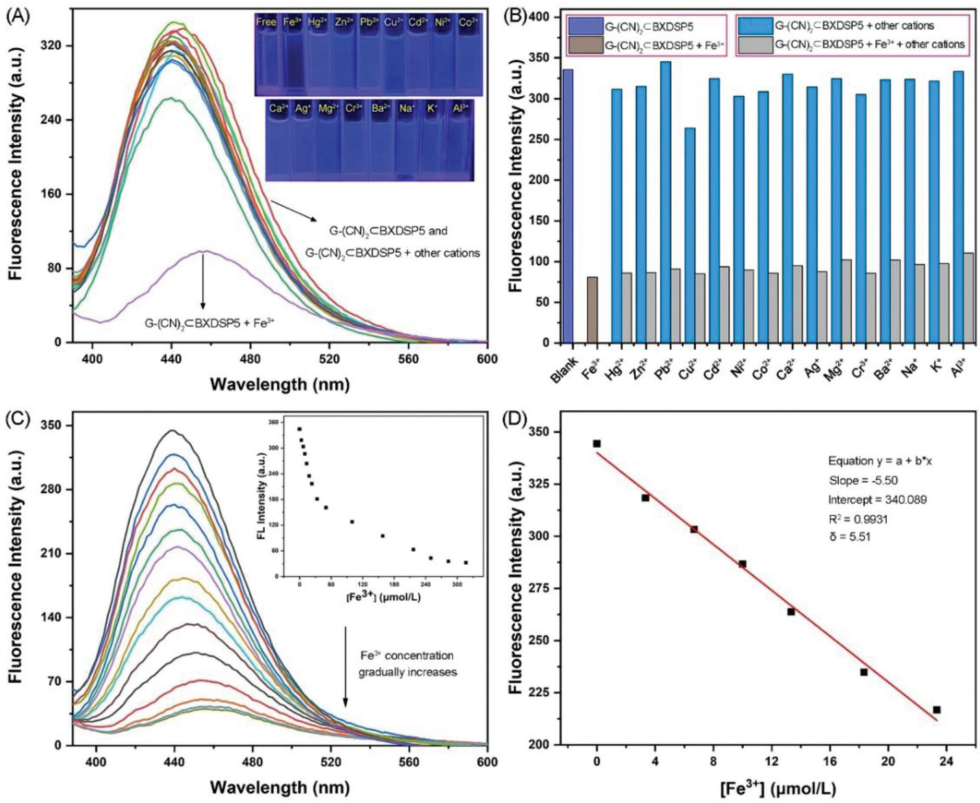

Fig. 4. (A) Fluorescence spectra for a mixture of G-$(CN)_2$⊂BXDSP5 and various cations. Inset: Fluorescence images of G-$(CN)_2$⊂BXDSP5 upon the addition of Fe^{3+}, Hg^{2+}, Zn^{2+}, Pb^{2+}, Cu^{2+}, Cd^{2+}, Ni^{2+}, Co^{2+}, Ca^{2+}, Ag^{+}, Mg^{2+}, Cr^{3+}, Ba^{2+}, Na^{+}, K^{+} and Al^{3+} (10 equiv.) excited at 365 nm at room temperature. (B) Fluorescence response of G-$(CN)_2$⊂BXDSP5 in the presence of various cations and Fe^{3+} (10 equiv.) at room temperature. (C) Fluorescence spectra of G-$(CN)_2$⊂BXDSP5 with increasing amounts of Fe^{3+}. Inset: A plot of fluorescence intensity at 440 nm *versus* concentrations of Fe^{3+}. (D) The linear relationship between the fluorescence intensity of G-$(CN)_2$⊂BXDSP5 at 440 nm and the concentration of Fe^{3+} (0–23.3 μmol/L) in DMSO-H_2O binary solutions (Experimental conditions: λ_{ex} = 365 nm; slit widths: Ex. 5 nm, Em. 5 nm; 298 K; [G-$(CN)_2$⊂BXDSP5] = 20 μmol/L; DMSO: H_2O = 1/9, v/v; correlation coefficient of 0.9931 (n = 20)).

G-$(CN)_2$⊂BXDSP5 showed a pronouncedly lower quantum yield (Φ) of 1.16% and fluorescence lifetime (τ) of 1.75 ns after the introduction of Fe^{3+}, along with an obvious lower radiative decay rate and higher non-radiative rate in comparison with individual G-$(CN)_2$⊂BXDSP5 (Figs. S33A and B, Table S4 in Supporting information). Anti-interference performance is one important parameter for sensing applications. To further explore the sensing selectivity and efficiency of G-$(CN)_2$⊂BXDSP5 toward Fe^{3+} over other cations, competitive experiments were conducted where equal equivalents of Fe^{3+} and other metal ions were added to the system. The fluorescence selectivity was studied at the emission maxima of 440 nm, and none of the competing metal ions showed obvious interference toward the quenching effect of the materials toward Fe^{3+} (Fig. 4B). This result further suggested that G-$(CN)_2$⊂BXDSP5 possessed high selectivity for Fe^{3+} without being interfered with by other competitive cations mentioned above.

Fluorescence titration experiments were performed to explore the efficiency of G-$(CN)_2$⊂BXDSP5 for detecting Fe^{3+}. Fluorescence of G-$(CN)_2$⊂BXDSP5 continued to quench with the increase of Fe^{3+} concentration (Fig. 4C), whereby fluorescence intensity increased rapidly under low concentrations of Fe^{3+} and then gradually reached a plateau. A good linear relationship between the emission intensity and the amount of Fe^{3+} within a range between 3.33 μmol/L and 23.33 μmol/L was achieved (Fig. 4D), with the limit of detection (LOD) calculated to be 3.0 μmol/L determined by the 3 δ/S method [47], endowing the supramolecular polymer with application potential in Fe^{3+} detection. Furthermore, the binding constant K_a between G-$(CN)_2$⊂BXDSP5 and Fe^{3+} was determined to be 7.40×10^4 L/mol by a linear fitting curve obtained from the fluorescence titration experiments (Fig. S34 in Supporting information).

Reversible fluorescence can also be achieved after the response toward Fe^{3+}. Since F^- is known to bind with Fe^{3+} ions to form stable $[FeF_6]^{3-}$ coordination complexes [48], the fluorescence intensity of the supramolecular polymer was successfully recovered upon the introduction of F^- (Fig. S35A in Supporting information). The appearance of a slight redshift at emission maxima was ascribed to the weak noncovalent interaction between triazole groups and excess fluoride anion [49]. After further adding Fe^{3+}, the fluorescence intensity of G-$(CN)_2$⊂BXDSP5 returned to the quenched state, designating the adjustable stimulus-responsive feature of the supramolecular polymer, and this switching could be progressed at least three cycles with minor loss in fluorescence efficiency (Fig. S35B in Supporting information).

We continued to study the quenching mechanism by Fe^{3+} toward the supramolecular polymer. First, UV-vis spectra of Fe^{3+} and emission spectra of G-$(CN)_2$⊂BXDSP5, where the absorbance of Fe^{3+} barely overlapped with the emission peak of G-$(CN)_2$⊂BXDSP5 (Fig. S36 in Supporting information), eliminating the possibility of dynamic quenching based on energy transfer [50]. Hence, we envision some other dominant factors responsible for the fluorescence change. Fourier transform infrared (FT-IR) spectroscopy, PXRD, SEM, and X-ray photoelectron spectroscopy (XPS) measurements were carried out. In the FT-IR spectra of G-$(CN)_2$⊂BXDSP5 before and after being treated with Fe^{3+}, the variation of stretching vibration absorption peaks of -C=O, -NH, and C-S-C groups suggests the coordination of Fe^{3+} with these motifs in G-$(CN)_2$⊂BXDSP5, resulting in the formation of G-$(CN)_2$⊂BXDSP5@Fe^{3+} (Fig. S37A in Supporting information). Moreover, in the PXRD pattern of G-$(CN)_2$⊂BXDSP5@Fe^{3+}, the stacking diffraction peak disappeared, indicating that π-π interactions were destroyed. Intriguingly, after adding F^- to G-$(CN)_2$⊂BXDSP5@Fe^{3+}, the peak at $2\theta = 22.73°$ reappeared (Fig. S37B in Supporting information). These findings verified that F^- can competitively bind with Fe^{3+}, and G-$(CN)_2$⊂BXDSP5 was released. The SEM image of G-$(CN)_2$⊂BXDSP5 after adding Fe^{3+} possessed irregular morphology distinct from the well-ordered three-dimensional microscale cubic structure of G-$(CN)_2$⊂BXDSP5 at the state of xerogel. Thus, we consider that the intermolecular hydrogen bonds and π-π interactions that contributed much to the network structure have been destroyed due to the coordination by Fe^{3+}. Synchronously, upon further addition of F^- to G-$(CN)_2$⊂BXDSP5@Fe^{3+}, the bulk structure reappeared (Figs. S38A–C in Supporting information), which is consistent with PXRD results. Furthermore, XPS spectra of G-$(CN)_2$⊂BXDSP5@Fe^{3+} showed a pronounced peak at 713 eV due to Fe 2p contribution (Fig. S39A in Supporting information), and the binding energy of Fe 2p (712.5 eV) was different from the peak at 711.5 eV of ferric chloride [51], where the slight increase of binding energy of Fe 2p was due to the formation of Fe-O bond in metal coordination complex G-$(CN)_2$⊂BXDSP5@Fe^{3+} (Fig. S39F in Supporting information) [52]. Meanwhile, the intensity of O 1s at 532.8 eV declines dramatically, demonstrating the change in oxygen-based species in the presence of Fe^{3+}. The binding energy of 530.8 eV originating from the C=O···metal coordination appeared upon adding Fe^{3+}, further verifying the coordination binding between carbonyl oxygens and Fe^{3+} (Fig. S39C in Supporting information) [53]. Additionally, the binding energy increase of N 1s and S 2p resulted from the formation of N···Fe and S···Fe coordination (Fig. S39D and S39E in Supporting information) [54–56]. In addition, Job's plot suggested that BXDSP5 and Fe^{3+} formed a 1:1 complex (Fig. S40 in Supporting information). The above results prove the metal coordination between G-$(CN)_2$⊂BXDSP5 and Fe^{3+}, and the proposed complexation mode of G-$(CN)_2$⊂BXDSP5 with Fe^{3+} is given in Scheme S3 (Supporting information).

The supramolecular polymer gel (G-$(CN)_2$⊂BXDSP5-G) was obtained at a phase-transition temperature of *ca.* 48–53 °C with the monomers at a concentration of 210 mmol/L in DMSO/$CHCl_3$ (v/v = 1/1). The solid-liquid balance (SLB) value of the resulting G-$(CN)_2$⊂BXDSP5-G was 0.33 (Fig. S41A in the Supporting information), signifying that the solid behaviors dominated the gelation. However, with the gradual addition of Fe^{3+} into the supramolecular gel, the SLB value increased and exceeded the critical value (0.5), which directly revealed the collapse of the supramolecular polymer gel [57]. This phenomenon further answers the Fe^{3+} recognition mechanism studied in the last section. Moreover, oscillatory sweep experiments were performed to obtain the rheological properties. The result showed that the frequency dependence of viscosity modulus G'' and elastic modulus G' of this supramolecular material, where G' was larger than G'' in the given scan range of frequency (Fig. S41B in Supporting information), indicating the stable gel state.

In the subsequent study concerning the stimuli-responsive properties of the gel, the reversible thermo- and mechanical force-induced gel-sol transitions of the polymer were visualized macroscopically (Fig. S42 in Supporting information). These desirable transformations can be explained by the fact that the dynamic host–guest interaction and hydrogen bonding within the supramolecular polymer networks are vulnerable to heating and vibrating, thus causing the decomplexation of the host–guest complexes and the destruction of the intermolecular hydrogen bonding interactions, leading to the disassembly of G-$(CN)_2$⊂BXDSP5-G. However, G-$(CN)_2$⊂BXDSP5-G also exhibited irreversible responsiveness toward the competitive guest, adiponitrile, since introducing adiponitrile into the solution of G-$(CN)_2$⊂BXDSP5 would cause the de-threading of G-$(CN)_2$ from the cavity of BXDSP5. Temperature-variant ^{1}H-NMR experiments of G-$(CN)_2$⊂BXDSP5 were performed to study the temperature-dependence of the supramolecular polymer gel (Fig. S43 in Supporting information), which proved that the host–guest complexation and intermolecular hydrogen bonding interactions were weakened as the temperature was raised. The above results suggested that G-$(CN)_2$⊂BXDSP5-

G possessed reversible gelation behaviors and favorable stimuli-responsive properties.

To examine the practical application potential of the fluorescent supramolecular polymer network G-$(CN)_2$⊂BXDSP5, a thin film of G-$(CN)_2$⊂BXDSP5 was prepared and utilized in visually detecting Fe^{3+}. As Fe^{3+} was used to write on the thin film, patterns due to the fluorescence quenching were observed under a UV lamp. Furthermore, fluorescence can be effectively regenerated as F^- was added. These results indicate that the G-$(CN)_2$⊂BXDSP5-based thin film could serve as a rewritable fluorescent material to detect Fe^{3+} (Fig. S44 in Supporting information).

In addition, the application of adsorbing Fe^{3+} from water by applying xerogel of G-$(CN)_2$⊂BXDSP5-based absorbent was also investigated, which displayed a remarkable Fe^{3+} adsorption efficiency of over 95% (Table S5 in Supporting information). Therefore, apart from fluorescent detection, this supramolecular polymer material also could effectively remove Fe^{3+} from water.

In this study, we have successfully designed and constructed a new supramolecular polymer network (G-$(CN)_2$⊂BXDSP5) based on the benzo[*f*]coumarin derivative-functionalized pillararene, which was associated with multiple non-covalent interactions including π-π stacking, hydrogen bonding, and host–guest interaction. The supramolecular polymer network showed excellent AIE properties with high photostability and quantum yields and sensing ability of Fe^{3+} with specific selectivity based on the strong complexation between Fe^{3+} and the host. Additionally, the supramolecular polymer could be further transformed into supramolecular gel under appropriate conditions, which displayed reversible sol-gel transitions initiated by different stimuli. Practical applications involving rewritable visual detection *via* thin films and effective adsorption of Fe^{3+} have also been realized. Considering the remarkable AIE property and exceptional sensing capability of the supramolecular polymer, the present study not only expands the scope of AIE supramolecular polymers but also provides a novel and simple strategy to fabricate stimuli-responsive supramolecular polymer materials for the detection and adsorption of metal ions for environmental applications.

Declaration of competing interest

The authors declare no conflicts of any financial interest.

Acknowledgments

The authors acknowledge the Jilin Province University Cooperative Construction Project-Special Funds for New Materials (No. SXGJSF2017-3) for financial support.

Supplementary materials

Supplementary material associated with this article can be found, in the online version, at doi:10.1016/j.cclet.2022.107877.

References

[1] D. Feng, T. Zhang, T. Zhong, et al., J. Mater. Chem. C 9 (2021) 16978–16984.
[2] Y. Luo, W. Zhang, Q. Ren, et al., Chin. Chem. Lett. 33 (2022) 5120–5123.
[3] M.K. Goshisht, G.K. Patra, N. Tripathi, Mater. Adv. 3 (2022) 2612–2669.
[4] Q. Yang, C. Li, J. Li, et al., J. Mater. Chem. C 8 (2020) 5554–5561.
[5] S.H. Park, N. Kwon, J.H. Lee, J. Yoon, I. Shin, Chem. Soc. Rev. 49 (2020) 143–179.
[6] L.J. Chen, Y.Y. Ren, N.W. Wu, et al., J. Am. Chem. Soc. 137 (2015) 11725–11735.
[7] H. Wang, X. Ji, Z. Li, F. Huang, Adv. Mater. 29 (2017) 1606117.
[8] Z. Zhao, H. Zhang, J.W.Y. Lam, B.Z. Tang, Angew. Chem. Int. Ed. 59 (2020) 9888–9907.
[9] J. Li, J. Wang, H. Li, et al., Chem. Soc. Rev. 49 (2020) 1144–1172.
[10] X. Zhao, Y. Chen, G. Niu, et al., ACS Appl. Mater. Interfaces 11 (2019) 13134–13139.
[11] C.W. Zhang, B. Ou, S.T. Jiang, et al., Polym. Chem. 9 (2018) 2021–2030.
[12] Y. Wang, M.Z. Lv, N. Song, et al., Macromolecules 50 (2017) 5759–5766.
[13] J. Wu, S. Sun, X. Feng, et al., Chem. Commun. 50 (2014) 9122–9125.
[14] Z.Y. Li, Y. Zhang, C.W. Zhang, et al., J. Am. Chem. Soc. 136 (2014) 8577–8589.
[15] Z. Li, G. Yu, J. Yang, Org. Chem. Front. 4 (2017) 115–118.
[16] W. Xia, M. Ni, C. Yao, et al., Macromolecules 48 (2015) 4403–4409.
[17] P. Wang, J. Ma, D. Xia, Org. Chem. Front. 5 (2018) 1297–1302.
[18] Y. Wang, C.L. Sun, L.Y. Niu, et al., Polym. Chem. 8 (2017) 3596–3602.
[19] X. Yan, F. Wang, B. Zheng, F. Huang, Chem. Soc. Rev. 41 (2012) 6042–6065.
[20] D. Chen, J. Zhan, M. Zhang, et al., Polym. Chem. 6 (2015) 25–29.
[21] Y. Li, Y. Dong, X. Miao, et al., Angew. Chem. Int. Ed. 57 (2018) 729–733.
[22] S. Guo, Y. Song, Y. He, X.Y. Hu, L. Wang, Angew. Chem. Int. Ed. 57 (2018) 3163–3167.
[23] J. Li, K. Shi, M. Drechsler, et al., Chem. Commun. 52 (2016) 12466–12469.
[24] H. Wang, X. Ji, Z. Li, et al., Mater. Chem. Front. 1 (2017) 167–171.
[25] N. Song, T. Kakuta, T. Yamagishi, Y.W. Yang, T. Ogoshi, CHEM 4 (2018) 2029–2053.
[26] M.H. Li, X.Y. Lou, Y.W. Yang, Chem. Commun. 57 (2021) 13429–13447.
[27] X.S. Hu, H.M. Deng, J. Li, X.S. Jia, C.J. Li, Chin. Chem. Lett. 24 (2013) 707–709.
[28] J.D. Ding, W.J. Jin, Z. Pei, Y. Pei, Chem. Commun. 56 (2020) 10113–10126.
[29] Y.F. Li, Z. Li, Q. Lin, Y.W. Yang, Nanoscale 12 (2020) 2180–2200.
[30] F. Lu, Y. Chen, B. Fu, S. Chen, L. Wang, Chin. Chem. Lett. 33 (2022) 5111–5115.
[31] K. Zhong, S. Lu, W. Guo, et al., J. Mater. Chem. A 9 (2021) 10180–10185.
[32] P. Li, Y. Chen, Y. Liu, Chin. Chem. Lett. 30 (2019) 1190–1197.
[33] D. Dai, Z. Li, J. Yang, et al., J. Am. Chem. Soc. 141 (2019) 4756–4763.
[34] Z. Liu, J. Wu, C. Wang, et al., Chin. Chem. Lett. 30 (2019) 2299–2303.
[35] X.H. Wang, N. Song, W. Hou, et al., Adv. Mater. 31 (2019) 1903962.
[36] X.Y. Lou, Y.W. Yang, Adv. Mater. 32 (2020) 2003263.
[37] T. Xiao, W. Zhong, L. Zhou, et al., Chin. Chem. Lett. 30 (2019) 31–36.
[38] X.Y. Lou, Y.W. Yang, Adv. Opt. Mater. 6 (2018) 1800668.
[39] X.H. Wang, X.Y. Lou, T. Lu, et al., ACS Appl. Mater. Interfaces 13 (2021) 4593–4604.
[40] X.Y. Lou, Y.W. Yang, J. Am. Chem. Soc. 143 (2021) 11976–11981.
[41] J. Yang, D. Dai, L. Ma, Y.W. Yang, Chin. Chem. Lett. 32 (2021) 729–734.
[42] X.Y. Lou, N. Song, Y.W. Yang, Chem. Eur. J. 25 (2019) 11975–11982.
[43] P. Wang, X. Yan, F. Huang, Chem. Commun. 50 (2014) 5017–5019.
[44] Y. Jia, J.P. Hu, L.R. Dang, et al., ACS Sustainable Chem. Eng. 9 (2021) 16203–16209.
[45] R. Zhang, X. Yan, H. Guo, et al., Chem. Commun. 56 (2020) 948–951.
[46] K.E. Feldman, M.J. Kade, E.W. Meijer, C.J. Hawker, E.J. Kramer, Macromolecules 43 (2010) 5121–5127.
[47] H.N. Kim, W.X. Ren, J.S. Kim, J. Yoon, Chem. Soc. Rev. 41 (2012) 3210–3244.
[48] Q. Lin, G.F. Gong, Y.Q. Fan, et al., Chem. Commun. 55 (2019) 3247–3250.
[49] G. Yu, Z. Zhang, C. Han, et al., Chem. Commun. 48 (2012) 2958–2960.
[50] W.M. Wang, D. Dai, J.R. Wu, et al., Chem. Eur. J. 27 (2021) 11879–11887.
[51] Y.I. Kim, W.E. Hatfield, Inorg. Chim. Acta 188 (1991) 15–24.
[52] J. Wang, Y. Fan, H.w. Lee, et al., ACS Appl. Nano Mater. 1 (2018) 3747–3753.
[53] X. Li, Z. Li, Y.W. Yang, Adv. Mater. 30 (2018) 1800177.
[54] W. Yan, C. Zhang, S. Chen, L. Han, H. Zheng, ACS Appl. Mater. Interfaces 9 (2017) 1629–1634.
[55] D. Ma, B. Li, Z. Cui, et al., ACS Appl. Mater. Interfaces 8 (2016) 24097–24103.
[56] S. Li, Y. Li, J. Cao, et al., Anal. Chem. 86 (2014) 10201–10207.
[57] H. Yao, X.T. Kan, Q. Zhou, et al., ACS Sustain. Chem. Eng. 8 (2020) 13048–13055.